Fatigue response up to 10^9 cycles of a structural epoxy adhesive

Fatigue response up to 10^9 cycles of a structural epoxy adhesive

Journal:	*Fatigue & Fracture of Engineering Materials & Structures*
Manuscript ID	FFEMS-8619
Manuscript Type:	Original Contribution
Date Submitted by the Author:	12-Feb-2020
Complete List of Authors:	Tridello, Andrea; Politecnico di Torino, Department of Mechanical and Aerospace Engineering Ciardiello, Raffaele; Politecnico di Torino, Department of Mechanical and Aerospace engineering Paolino, Davide S.; Politecnico di Torino, Department of Mechanical and Aerospace Engineering Goglio, Luca; Politecnico di Torino, Department of Mechanical and Aerospace Engineering

Highlights

1. Ultrasonic fatigue tests on structural adhesives can be reliably performed.

2. Surface defects are detrimental for the VHCF response of adhesives.

3. Internal defects have limited influence on the VHCF response of adhesives.

4. Fracture surfaces of adhesives subjected to VHCF loads show a peculiar morphology.

Fatigue response up to 10^9 cycles of a structural epoxy adhesive

Authors:
A. Tridello[a], R. Ciardiello[b], D.S. Paolino[c], L. Goglio[d]

[a] Department of Mechanical and Aerospace Engineering, Politecnico di Torino, 10129 Turin, Italy, andrea.tridello@polito.it
[b] Department of Mechanical and Aerospace Engineering, Politecnico di Torino, 10129 Turin, Italy, raffaele.ciardiello@polito.it
[c] Department of Mechanical and Aerospace Engineering, Politecnico di Torino, 10129 Turin, Italy, davide.paolino@polito.it
[d] Department of Mechanical and Aerospace Engineering, Politecnico di Torino, 10129 Turin, Italy, luca.goglio@polito.it

Corresponding Author:
A. Tridello
E-mail address: andrea.tridello@polito.it
Full postal address:
C.so Duca degli Abruzzi 24,
Department of Mechanical and Aerospace Engineering – Politecnico di Torino,
10129 – Turin,
ITALY
Phone number: +39.011.090.6913
Fax number: +39.011.090.6999

Abstract:

In the present paper, the Very-High-Cycle-Fatigue (VHCF) response of a structural adhesive used for automotive applications, Betaforce 4600G modified with microspheres, has been experimentally assessed. Ultrasonic fully reversed tension-compression tests up to 10^9 cycles have been carried out with the testing machine developed by the Authors on adhesives without macroscopic defects and on adhesives with artificial defects, inserted during the butt-joint preparation. Fracture surfaces have been observed with the optical microscope and the P-S-N curves estimated. Experimental results have shown that defect location significantly affects the VHCF strength and fracture surfaces exhibit a peculiar morphology with three distinct characteristic regions.

Keywords: Very-High-Cycle Fatigue (VHCF); ultrasonic fatigue tests; accelerated tests; structural adhesive; epoxy resin.

Acronyms and nomenclature

c_Y, m_Y: constant coefficients.

E_{ad}, η_{ad}: Young's modulus and loss factor of the adhesive.

$E_{ad,FEA}$, $\eta_{ad,FEA}$: Young's modulus and loss factor of the adhesive for the FEA model.

FEA: Finite Element Analysis

L_{tot}: length of the adhesive butt-joint specimen

L_1: length of adherend 1;

L_2: length of adherend 2:

L_{ad}: adhesive thickness.

s_{min}, s_{max} : minimum and maximum stress amplitude within the adhesive.

s_{exp} , s_{FEA}: stress amplitude within the adhesive experimentally measured and computed through FEA.

SEM: Scanning Electron Microscope

VHCF: Very High Cycle Fatigue

x: logarithm of the applied stress amplitude.

$\mu_Y(x)$: mean of the fatigue life distribution

σ_Y: standard deviation of the fatigue life distribution

1. INTRODUCTION

In the last years, the research on lightweight design of components has become a major topic for universities and industries. For example, in the automotive, marine, and aerospace sectors[1-3], the reduction of the vehicle weight is of primary importance due to the stringent regulations in terms of fuel consumption and emissions[4], which have given a significant boost to the use of lightweight materials (e.g., composite materials[5, 6]) or to the development of new design and manufacturing processes allowing to produce light components with optimized mass distribution (e.g., topology optimization and Additive Manufacturing). At the same time, it has been demonstrated that a further significant reduction of the weight of mechanical structures and vehicles can be achieved with structural adhesives for joining different components[6]. Indeed, the replacement of traditional joining techniques and mechanical fasteners with structural adhesives contributes to the reduction of the weight of mechanical assemblies, without affecting the mechanical strength and the stiffness of the joint. In particular, the use of adhesives simplifies the manufacturing process and, above all, structural adhesives are preferred to traditional joining techniques for their high strength to weight ratio, for their capacity to join dissimilar materials that can be hardly joined with other techniques and to improve the stress distribution and the stress uniformity along the lap region[1, 7-8]. The mechanical characterization of structural adhesives under different loading conditions has thus become fundamental to guarantee a safe design for the joint and is therefore of utmost interest for researchers and industries.

Among structural adhesives, epoxy-based adhesives are widely used in the automotive sector for their ability to bond a wide range of materials, even dissimilar[9]. These adhesives are available in two-component (resin and hardener) products which can be cured at room temperature and in mono-component products that need elevated temperature for the activation. As for other structural components, they are subjected to different types of loads and, accordingly, to different failure modes: in particular, fatigue loads are extremely dangerous. A proper experimental characterization of the fatigue response of the adhesive is therefore mandatory to prevent the failure of the joint. According to the literature[10, 11], fatigue tests on adhesives are typically interrupted at 10^7 cycles (runout number of cycles), since they are in almost all the cases carried out with traditional testing machines (e.g., electro-hydraulic[10]) working at a loading frequency smaller than 100 Hz. Due to a significantly large testing time, the Very-High-Cycle Fatigue (VHCF) region (i.e., the fatigue region beyond 10^7 cycles) is instead rarely assessed. However, as for other structural components, the required fatigue lifetime of adhesives has significantly increased in the last years. For example, the fatigue life of components and, accordingly of the joints between components, could exceed 10^9 cycles in automotive and aerospace applications[12, 13], mainly due to the loads induced by low amplitude vibrations[13]. For these reasons and for a conservative design of joints employed for critical structural applications, fatigue tests cannot be limited to 10^7 cycles and the VHCF response of adhesives should be properly experimentally assessed.

In the present paper, the VHCF response of a structural adhesive used for automotive applications, Betaforce 4600G modified with microspheres for the thickness control ($200\ \mu m$), has been experimentally assessed. Ultrasonic (loading frequency of $20\ kHz$) fully reversed tension-compression tests up to 10^9 cycles have been carried out by using the ultrasonic testing machine developed at Politecnico di Torino. In particular, the ultrasonic testing machine for VHCF tests on metal materials[14, 15] has been adapted to perform accelerated tests on adhesive butt-joints[16]. Fatigue tests have been carried out on adhesives without macroscopic defects and on adhesives with artificial surface and internal defects, inserted during the butt-joint preparation, with the aim of investigating the effect of defect size and location on the crack nucleation and on the VHCF response. Fracture surfaces have been observed with the optical microscope and, finally, the P-S-N curves estimated.

2. MATERIALS AND METHODS

The present Section describes the experimental activity. In Subsection 2.1, the adhesive characteristic and the butt-joint design procedure are reported. In Subsection 2.2, the system developed to prepare the butt-joint is described. In Subsection 2.3, the methodology developed by the Authors for the assessment of the Dynamic Elastic Modulus and the loss factor of the adhesive is reported. In Subsection 2.4, the ultrasonic fatigue testing configuration and the control system are described in detail. In the following, "adhesive butt-joint specimen" will refer to the specimen obtained by bonding together the two Ti6Al4V round bars with the Betaforce 4600G adhesive.

2.1. Adhesive butt-joint specimen: design

The tested adhesive, Betaforce 4600G (supplied by Dow Automotive), is a mono-component adhesive that has been modified by the manufacturer with glass spheres to maintain the adhesive thickness close to the optimal value of $200\ \mu m$. The microsphere diameter has been verified with the Scanning Electron Microscope (SEM). Table 1 reports the adhesive mechanical properties taken from the datasheet provided by the adhesive manufacturer.

Betaforce 4600G datasheet	
Tensile strength	56 MPa
Elastic modulus	2900 MPa
Lap shear strength (thickness 0.2 mm)	26 MPa
Elongation at break	4%

Table 1: Betaforce 4600G mechanical properties reported on the datasheet provided by the adhesive manufacturer.

The adhesive butt-joint subjected to the fatigue test has been obtained by bonding together two Ti6Al4V round bars with calibrated lengths. The lengths have been defined through a procedure developed by the Authors and based on Finite Element Analysis (FEA)[16]. In particular, the lengths L_1 and L_2 (length of adherend 1 and 2, respectively) are designed to meet the resonance condition: the adhesive butt-joint specimen, characterized by a total length $L_{tot} = L_1 + L_2 + L_{ad}$ (being L_{ad} is the adhesive thickness) must have the same resonance frequency of the system piezoelectric transducer-booster-horn in the ultrasonic testing machine. The second condition for defining the lengths L_1 and L_2 concerns the desired stress amplitude range, [s_{min}; s_{max}], to be applied to the adhesive. Indeed, by varying the lengths L_1 and L_2 (and therefore the relative position of the adhesive joint within L_{tot}) it is possible to vary to applied stress amplitude range within the adhesive. More details on the design procedure and on the characteristic of the adhesive butt-joint specimen can be found in Ref.[16].

For testing the Betaforce 4600G adhesive, the same adhesive butt-joint specimen geometry adopted in Ref.[16] (Ti6Al4V round bar diameter of 14.6 mm, $L_1 = 114.25$ mm and $L_2 = 7.7$ mm) has been considered in this study. Since the thickness and the dynamic elastic modulus of the tested adhesive are different from those of the cyanoacrylate adhesive tested in Ref.[16], a FEA calibration of the applied stress amplitude within the adhesive has been carried out. An FE model of the adhesive butt-joint specimen and the horn has been created according to Ref.[16]. The mechanical properties of the Ti6Al4V bars used for the joint correspond to those reported in Ref.[16]; whereas, the Young's modulus and the loss factor of the Betaforce 4600G adhesive have been experimentally assessed (Section 2.3). According to Ref.[16], a harmonic analysis has been carried out by applying a harmonic force at the horn end (i.e., where the horn is connected to the system piezoelectric transducer/booster), in order to correlate the horn input displacement and the applied stress amplitude within the tested adhesive. For the tested adhesive, the stress range is $[5.9{:}51.6]$ MPa.

2.2. Adhesive butt-joint: joint preparation

The adhesive butt-joint specimens have been prepared by using a device (Fig. 1) developed by the Authors and following the Betaforce supplier indications, in order to obtain the maximum bonding strength. Firstly, a superficial pre-treatment has been carried out to remove contaminants: the surfaces have been cleaned with sandpaper and then the residue of the polishing process has been removed with acetone. The application of the adhesive has been performed at a temperature of $60°$ C to reduce its viscosity which is relatively high at room temperature (230 Pa·s). At $60°$ C the viscosity is lower enough so that the adhesive can be easily spread on the adherend through a nozzle. The device shown in Fig. 1 has been used for maintaining the proper bonding pressure during the curing process (180 °C for 30 minutes), as specified by the supplier.

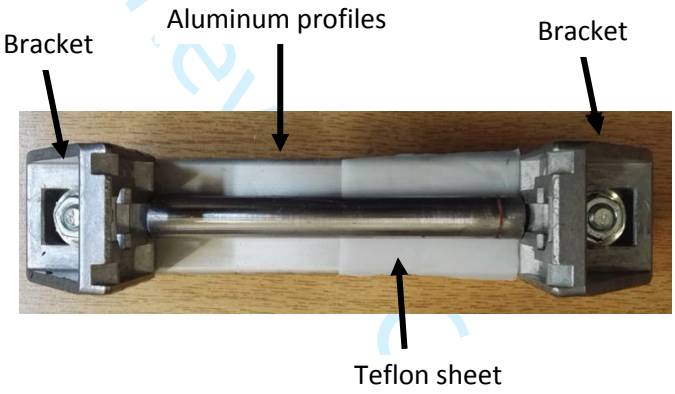

Figure 1: Device used for the preparation of the adhesive butt-joint specimens in order to maintain the proper bonding pressure during the curing process.

Eighteen adhesive butt-joint specimens have been tested. Three adhesive butt-joint specimens with "artificial defects" have been also tested in order to investigate the effect of improper bonding and of defect location on the VHCF strength. The artificial defects have been created by placing thin Teflon sheets (thickness smaller than 100 μm) on one of the two adherends, thus creating small regions without adhesive and, therefore, artificial defects. Three cases, schematically shown in Fig. 2, have been investigated: adhesive with a surface defect (Fig. 2a), adhesive with an internal defect (Fig. 2b) and adhesive with surface and internal defects (Fig. 2c). The real size of the artificial defects has been accurately measured on the fracture surface images obtained with an optical microscope.

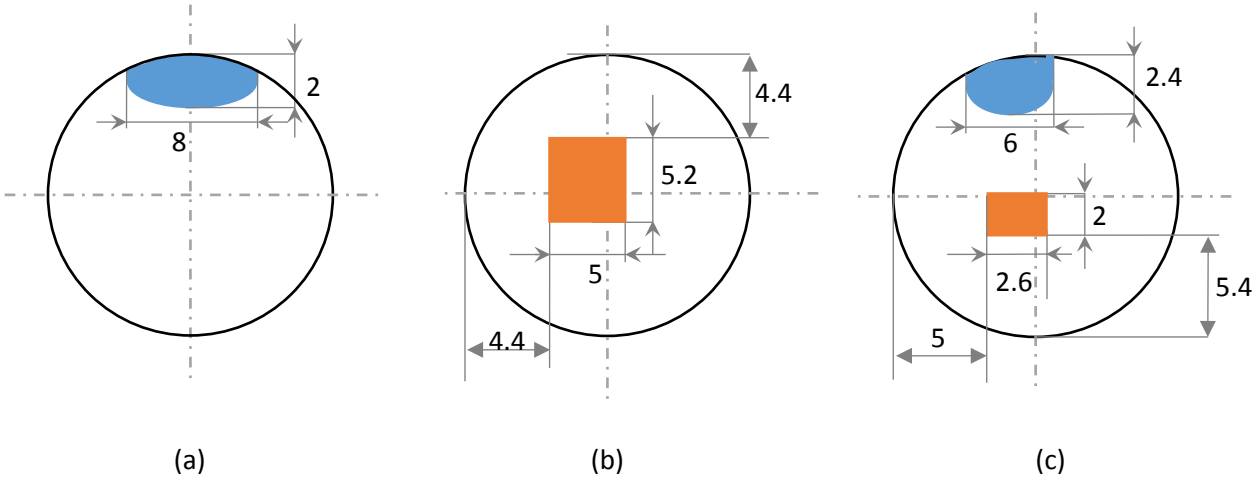

Figure 2: Location and geometry of the artificial defects: a) surface defect; b) internal defect; c) surface and internal defects.

2.3 Dynamic properties

The adhesive dynamic properties (dynamic Young's modulus, E_d, and loss factor, η_{ad}), which are necessary for the assessment of the stress amplitude within the adhesive through FEA, have been estimated with the iterative experimental-FEA procedure shown in Fig. 3. In particular, Fig. 3a) and Fig. 3b) show the iterative procedure developed for estimating E_{ad} and η_{ad}, respectively.

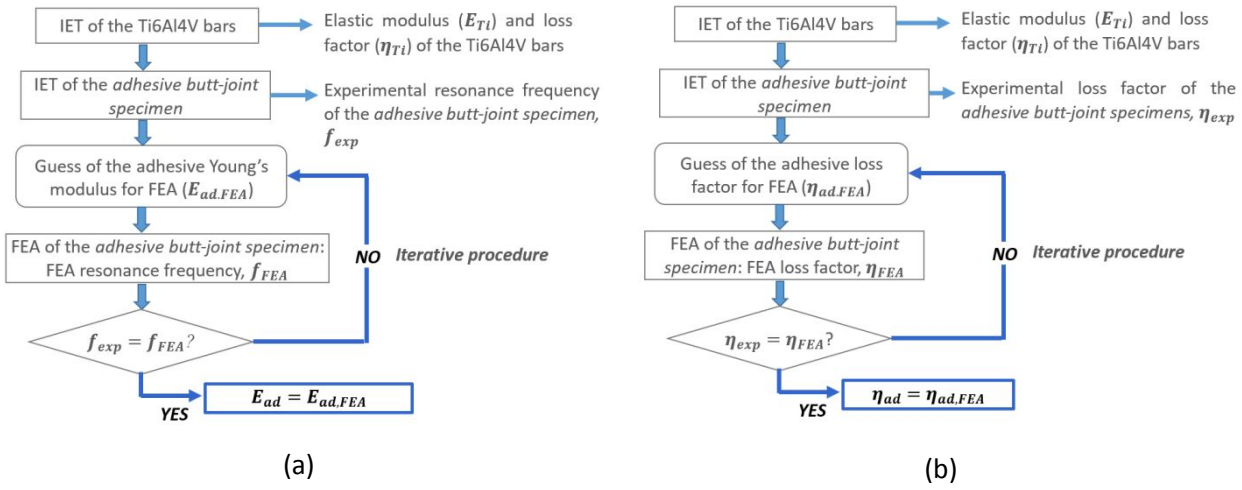

Figure 3: Flow chart of the iterative procedure developed to estimate the adhesive elastic properties: a) dynamic Young's modulus, E_{ad}; b) loss factor, η_{ad}.

According to Fig. 3a), the first step involves the experimental assessment of the dynamic elastic modulus and of the loss factor for the Ti6Al4V adherends[16], through the Impulse Excitation Technique[17] (IET). Thereafter,

the two Ti6Al4V adherends are bonded together and the longitudinal resonance frequency (f_{exp}) of the adhesive butt-joint specimen is measured again with the IET. Following the flow chart in Fig. 3a), a FE model of the adhesive butt-joint specimen is then created and its first longitudinal resonance frequency, f_{FEA}, is obtained with a modal analysis. For the first iteration, a tentative value of 1 GPa for the dynamic Young's modulus, $E_{ad,FEA}$, and of $3.4 \cdot 10^{-3}$ for the loss factor, $\eta_{ad,FEA}$, have been considered for the FEA model[16]. The experimental resonance frequency f_{exp} is finally compared with the FEA resonance frequency, f_{FEA}: according to Fig. 3a), if the two values do not match, $E_{ad,FEA}$ is iteratively varied until the condition $f_{exp} = f_{FEA}$ is met. When $f_{exp} = f_{FEA}$, the FEA Young's modulus corresponds to the actual adhesive Young's modulus ($E_{ad,FEA} = E_{ad}$), which has been found to be equal to 3.1 GPa. The same procedure has been repeated to estimate the adhesive loss factor (Fig. 3b): in this case, the condition that has been met is $\eta_{exp} = \eta_{ad,FEA}$, being η_{exp} and $\eta_{ad,FEA}$ the experimental and the FEA loss factors of the adhesive butt-joint, respectively. The *half-power bandwidth method*[18] has been applied for assessing η_{exp} and $\eta_{ad,FEA}$: when $\eta_{exp} = \eta_{ad,FEA}$, the FEA loss factor corresponds to the actual adhesive loss factor ($\eta_{ad,FEA} = \eta_{ad}$), which has been found to be equal to $2 \cdot 10^{-2}$. It is worth to note that, by varying $\eta_{ad,FEA}$ during the iterative procedure, f_{FEA} could vary (i.e., E_{ad} should be also varied to meet again the condition $f_{exp} = f_{FEA}$). However, it has been verified that, for the investigated range of the loss factor, the variation of f_{FEA} with respect to $\eta_{ad,FEA}$ was negligible.

2.4 Experimental tests

Before the ultrasonic fatigue tests, three tensile tests have been carried out on adhesive butt-joint specimens. In this case, however, the length of the adherends has been increased to 60 mm in order to properly grip the tested specimens. A servo-hydraulic testing machine, Instron 8801, has been used for the tests, with a crosshead displacement rate of 2 mm/min.

Fully reversed ultrasonic tension-compression tests at constant amplitude have been carried out on the Betaforce 4600G adhesive butt-joints with the ultrasonic fatigue testing machine developed by the Authors for tests on metallic materials[14-15]. The metal specimen commonly tested (hourglass, dogbone or Gaussian specimen) has been replaced by the adhesive butt-joint specimen. Fig. 4 shows the testing system developed by the Authors: the adhesive butt-joint specimen, the strain gage used for the calibration of the FEA model (calibration gage in Fig. 4), and the sensors used for measuring the displacement amplitude (laser displacement sensor in Fig. 4) and the temperature (infrared temperature sensor in Fig. 4).

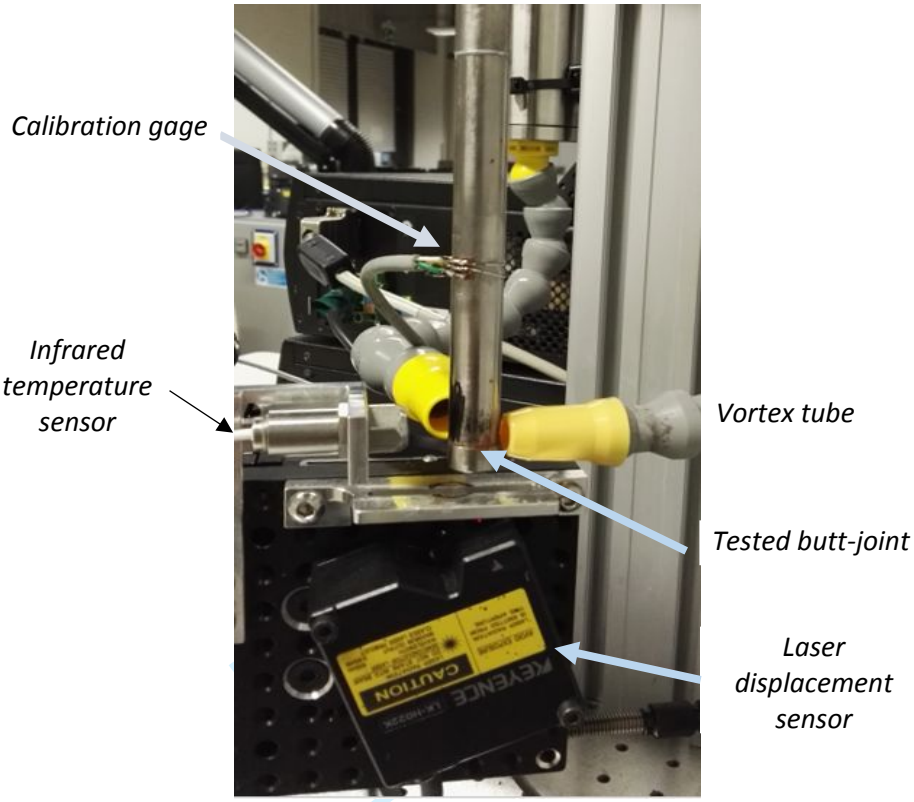

Figure 4: Ultrasonic fatigue testing system for VHCF tests on adhesive butt-joints.

As shown in Fig. 4, a calibration strain gage rosette has been attached at the half length of the adhesive butt-joint specimen (L_{tot}) in order to validate the FEA model. The strain amplitude at the half of the adhesive butt-joint specimen length has been measured at increasing values of the input displacement provided by the piezoelectric transducer (displacement range $[1.1 - 1.5]$ μm). As in Ref.[16], a linear relationship between the input displacement and the strain amplitude has been found. For the same input displacement, the strain measured with the calibration gage, s_{exp}, has been compared with the strain computed through FEA, s_{FEA}. Similarly to Ref.[16], the difference between s_{exp} and s_{FEA} has been found to be very limited (smaller than 1%), thus proving that the stress amplitude within the adhesive can be reliably computed through FEA.

Ultrasonic tests have been carried out at constant stress amplitude: the applied stress amplitude within the adhesive has been kept constant through a closed-loop proportional feedback control based on the displacement amplitude measured with the laser sensor shown in Fig. 4 (KEYENCE LK-G5000, sample frequency of 300 kHz). The correlation between the measured displacement and the stress amplitude within the adhesive has been finally assessed through FEA.

The specimen temperature has been also monitored during the tests: in particular, the temperature measured as close as possible to the adhesive with an infrared temperature sensor (OPTRIS CT-LT-15) has been limited to a maximum value of $22°$ C. Two vortex tubes (Fig. 4) with the cold air flux concentrated near the adhesive have been also used to limit the adhesive heating during the test[15]. As shown in Ref.[16], by

limiting the temperature to 22° C near the joint, it is possible to keep the temperature inside the adhesive almost constant, with a limited increment during the test (less than 9% with respect to the initial value). For the largest applied stress amplitude, the temperature has exceeded the upper limit value of 22° C: in these cases, the control system automatically interrupts the test until the temperature drops below a lower limit set equal to $21\ ^\circ\ \mathrm{C}$ (intermittent testing condition[19, 20]).

3. EXPERIMENTAL RESULTS

Section 3 presents the experimental results. In Section 3.1 and in Section 3.2, the results of the tensile tests and of the ultrasonic tests are reported and analyzed. In Section 3.3, the fracture surfaces are analyzed and, finally, in Section 3.4 the P-S-N curves are estimated and a possible solution for the design curves is proposed.

3.1. Quasi-static tests

Figure 5a) and Fig. 5b) show the average stress-displacement curve and the fracture surfaces obtained through the tensile tests, respectively.

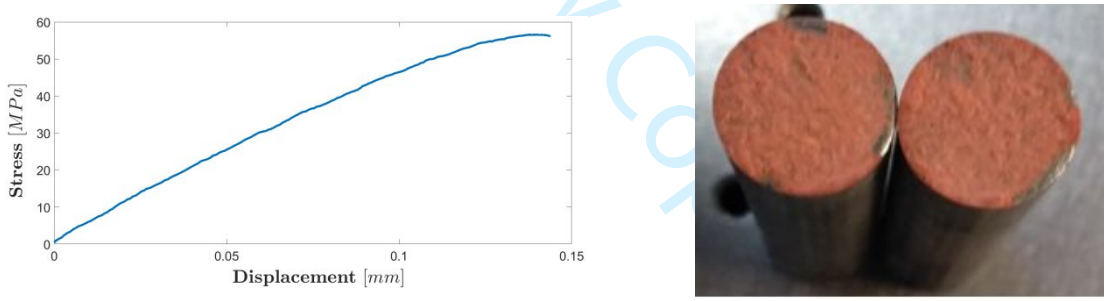

a b

Figure 5: Tensile test results: a) average stress displacement curve; b) fracture surface images.

According to Fig. 5 a), the average tensile strength is equal to $56\ \mathrm{MPa}$, in agreement with literature results on high strength structural epoxy adhesive[21]. The scatter of the tensile strength between the three tests is limited and smaller than 0.5%, proving the effectiveness of the procedure developed for the preparation of the adhesive butt-joint.

3.2. VHCF tests

Eighteen ultrasonic fatigue tests have been carried out on specimens without defects. Thirteen specimens have failed between $8.75{\cdot}10^5$ cycles and $2.57{\cdot}10^8$ cycles, in a stress range between $16\ \mathrm{MPa}$ and $26\ \mathrm{MPa}$,

and five specimens have not failed up to 10^9 cycles (runout specimens). The specimens with artificial defects have been tested at stress amplitudes in the range $[13 - 17]$MPa and failed between $1.85{\cdot}10^7$ cycles and $1.38{\cdot}10^8$ cycles. More in details, the specimen with the internal defect has been firstly tested at 13 MPa, but it has survived up to 10^9 cycles; it has been subsequently tested at 15 MPa, but, again, it has survived up to 10^9 cycles; it has been finally tested at 17 MPa and it has failed before 10^9 cycles. The specimens with artificial surface defects, on the contrary, have been tested at 13 MPa and have failed before 10^9 cycles.

Fig. 6 shows the experimental dataset in an S-N plot: both failures from specimens without defects and failures from specimens with artificial defects are reported.

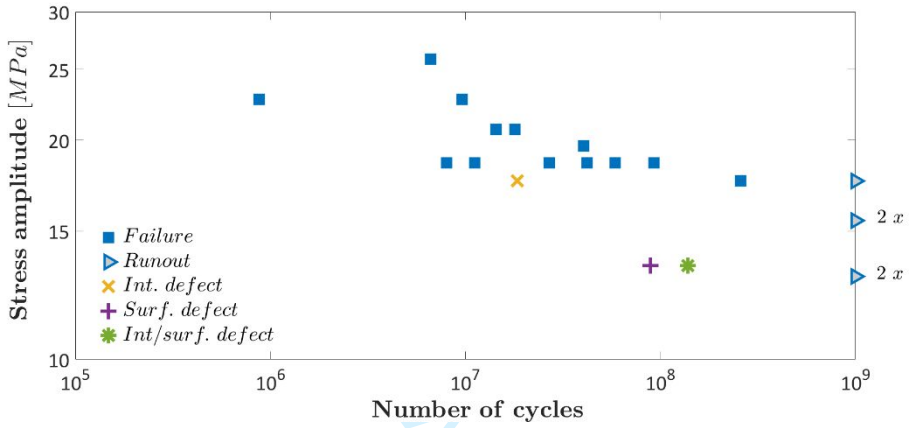

Figure 6: S-N plot of the experimental dataset.

Fig. 6 confirms that the proposed ultrasonic testing methodology can be effectively used for the assessment of the VHCF response of structural epoxy adhesives with thickness up to 200 μm. More in detail, all the fatigue failures originating in specimens without defects are at levels of stress amplitude above 16 MPa. Therefore, a conservative stress amplitude of 15 MPa can be considered as reference value for preventing failures within the adhesive at 10^9 cycles. On the other hand, by considering the specimens with artificial defects, the defect location clearly affects the VHCF strength. The specimens with an artificial surface defect are characterized by a significantly smaller VHCF strength: for examples, the specimens with surface defects have failed at 13 MPa, whereas, below 16 MPa, no failures have been found for specimens without defects. The internal defect is instead not detrimental for the VHCF response. The specimen with the internal defect has failed at 17 MPa at $1.85{\cdot}10^7$ cycles, with a VHCF strength close to the VHCF strength of specimens without defects.

3.3. Fracture surfaces

The fracture surfaces of all the failed specimens have been observed with the optical microscope. Fig. 7 shows a typical fracture surface for the specimens without artificial defects: Fig. 7a) and Fig. 7b) show the two adherends of the same tested specimen.

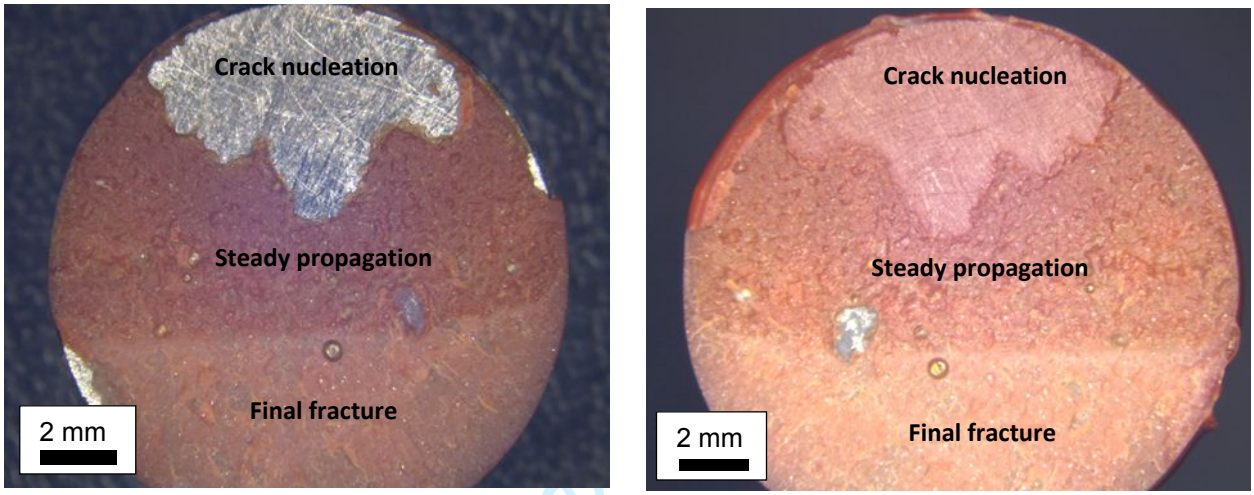

(a) (b)

Figure 7: Typical fracture surface for specimens without artificial defects: a) adherend 1; b) adherend 2.

Three distinct regions, characterized by different morphologies, can be clearly observed on the fracture surfaces:

- *Crack nucleation region*: in this region, the crack originates in proximity of the specimen free surface. The fracture surface shows an interfacial nature: as shown in Fig. 7a, the metal surface of adherend 1 is clearly visible.
- *Steady propagation*: in this region, the fracture surface shows a cohesive nature and the adhesive is visibly darker on the fracture surface. The maximum extension of this region corresponds to the size of the crack that causes the interruption of the test due to a significant reduction of the resonance frequency of the specimen (i.e., the test is interrupted if the resonance frequency of the specimen drops below $19450\ \mathrm{Hz}$).
- *Final failure*: this region, of cohesive nature, is characterized by a lighter colour than that in the second zone and is similar to that obtained in the quasi-static tests (Fig. 5b).

The fracture surfaces of the specimens with artificial defects have been also observed with the optical microscope. For one of the two adherends, Fig. 8a) shows the fracture surface of the specimen with

internal defect, Fig. 8b) shows the fracture surface of the specimen with surface defect and Fig. 8c) shows the fracture surface of the specimen with surface and internal defect.

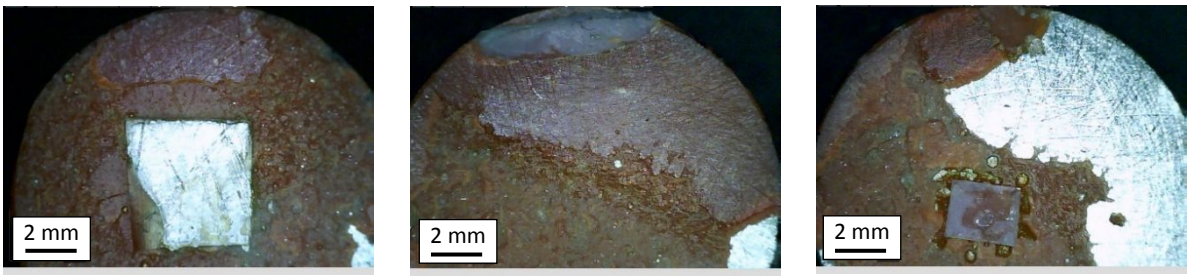

(a) (b) (c)

Figure 8: Fracture surfaces of specimens with artificial defects: a) specimen with internal defect: b) specimen with surface defect; c) specimen with surface and internal defects.

For the specimens with surface defects (Fig. 8b and Fig. 8c), the crack starts propagating from the artificial defect: in this region, the morphology is similar to the morphology of the region "Nucleation region" in Fig. 7. On the contrary, in the specimen with the internal artificial defect (Fig 8a), the fatigue crack does not start propagating from the defect, but it still originates from the specimen surface, with the fracture surface similar to that of specimens with no artificial defects. It is worth to note that, as shown in Ref.[16], even if small regions without adhesive and characterized by an imperfect bonding (simulated in Ref.[16] by randomly separating the nodes at the interface between the adhesive and the adherends) are present, the applied stress amplitude within the adhesive layer is only locally altered in the vicinity of the defect. This is confirmed by the fact that, even though an internal defect is present, the crack starts propagating from the surface (the weakest region) with a VHCF strength similar to that of specimens without defects.

The fracture surfaces have been also observed with the Scanning Electron Microscope (SEM). A Zeiss SUPRA40 Field Emission-SEM has been used, by considering an accelerating voltage of 10 kV with a secondary emission signal. The fracture surfaces have been coated with a gold layer of $10\ \mathrm{nm}$. Fig. 9 displays SEM images at different magnification of one representative fracture surface. In Figs 9a), 9b) and 9c), the steady propagation region is shown at three magnifications, 100x, 500x, and 1000x, respectively; whereas Figs 9d) and 9e) display the final fracture region observed at a magnification of 100x and 500x, with a detail of a microsphere in Fig. 9e).

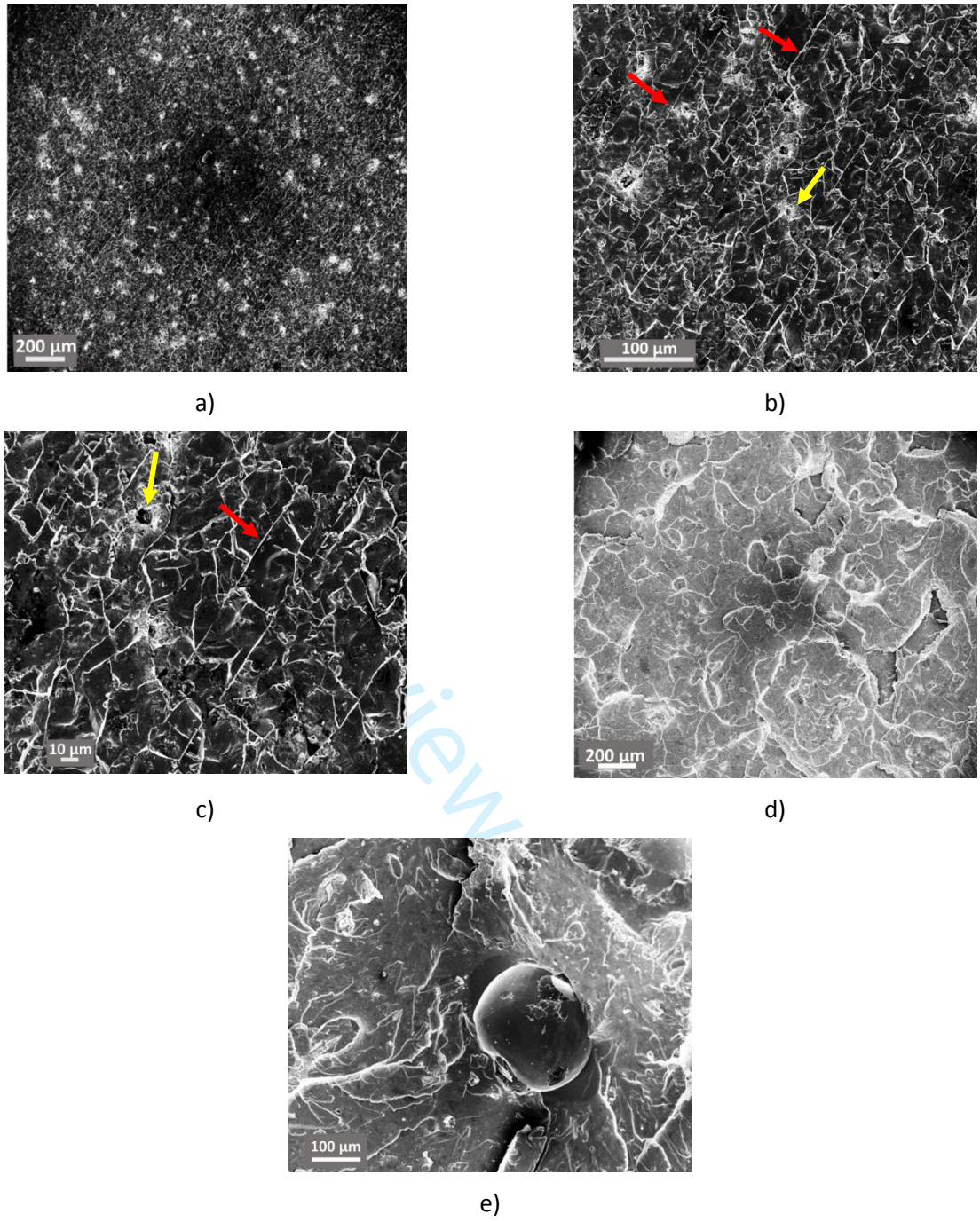

Figure 9: SEM images of the fracture surface: a) steady propagation region at 100x magnification; b) steady propagation region at 500x magnification; c) steady propagation region at 1000x magnification; d) final fracture region at 100x magnification; e) details of a microsphere in the final fracture region (500x).

Fig. 9a) shows that the morphology in the region of steady propagation is uniform. In Fig. 9b) and 9c), obtained at higher magnification, more details on the crack propagation region can be observed: in particular, the red arrows indicate areas of possible delamination and signs of crack propagation; whereas, the yellow arrows highlight micro-voids, with an average size of 10 µm, formed during the crack propagation or during the joint preparation. The same features, micro-voids and propagation lines, are not present in the region of

final fracture, shown in Fig. 9d). Figure 9e) shows a detail of a microsphere: the diameter has been measured and found to be equal to 200 μm, as declared by the adhesive supplier.

3.4. P-S-N curves

The P-S-N curves have been finally estimated. According to the literature (consider, for example, Reference[22] and the references therein), the logarithm of fatigue life is assumed to follow a Normal distribution with constant standard deviation, σ_Y, and mean that linearly depends on the applied stress amplitude ($\mu_Y(x) = c_Y + m_Y \cdot x$, being x the logarithm of the applied stress amplitude and c_Y and m_Y constant coefficients). The constant parameters of the distribution have been estimated by considering only specimens without artificial defects and by applying the Maximum Likelihood Principle in order to take into account both failures and runouts.

Fig. 10 shows the estimated median, the 0.95-th, 0.05-th and 0.01-th quantiles of the P-S-N curves, together with the experimental data. The VHCF response of the specimens with artificial defects are also reported on the P-S-N plot.

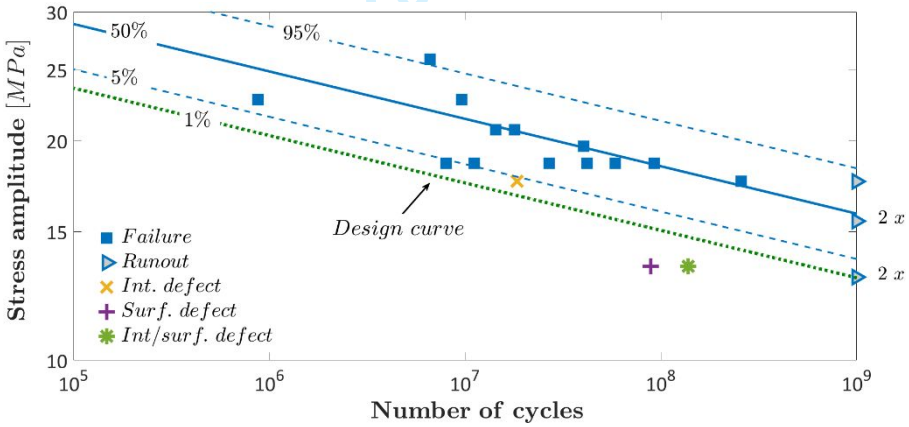

Figure 10: P-S-N curves (median, 95%, 5% and 1%) estimated from failures without defects.

According to Fig. 10, the estimated P-S-N curves are in good agreement with the experimental data: seven failures out of thirteen (about 50%) are below the median curve (Fig. 10). Furthermore, twelve failures out of thirteen are within the estimated 90% confidence interval, confirming that the statistical model is appropriate both for epoxy adhesives and for metallic materials[22]. The 1% probability P-S-N curve is below all the experimental failures of specimens without artificial defects and, therefore, can be conservatively considered as a design curve[14] for butt-joints with the Betaforce 4600G structural adhesive. Moreover, the P-S-N curves confirms the influence of defect location on the VHCF strength. The failure associated to the specimen with the artificial internal defect is slightly below the estimated 5% P-S-N curve, but conservatively above the 1% design curve, thus confirming that internal defects are less detrimental. On the contrary, the

two failures with surface artificial defects are significantly below the design curve. Therefore, it can be concluded that the 1% P-S-N curve can be used as design curve provided that large surface defects are not present in the butt-joints. On the contrary, in case of butt-joints with large surface defects, the fatigue strength is significantly lowered, with possible premature and dangerous failures even for very low stress amplitudes.

4. CONCLUSIONS

In the present paper, the VHCF response up to 10^9 cycles of a structural adhesive for automotive applications, epoxy Betaforce 4600G adhesive modified with microsphere of $200\ \mu m$ diameter for the thickness control, was experimentally assessed. Fully reversed tension-compression ultrasonic fatigue tests (working frequency of $20\ kHz$) were carried out on butt-joints obtained by bonding two Ti6Al4V bars with the investigated adhesive. The ultrasonic testing machine developed by the Authors for testing adhesives was used for the experimental tests.

Eighteen tests were carried on adhesive butt-joint specimens with no large macroscopic defects within the adhesive. Thirteen specimens failed between $8.75 \cdot 10^5$ e $2.57 \cdot 10^8$ cycles in a range of applied stress amplitude between 16 and $26\ MPa$. No failures occurred at levels of stress amplitude below $16\ MPa$. Therefore, a conservative stress amplitude of $15\ MPa$ was considered as reference value for preventing failures within the tested adhesive at 10^9 cycles.

Three tests were also carried out on adhesive butt-joints with large artificial defects within the adhesive. A significant dependence between the VHCF strength and the defect location was found: specimens with artificial surface defects were characterized by a VHCF strength significantly smaller (failures occurred at 13 MPa) than that of specimens without artificial defects. On the other hand, the specimen with the internal defect was characterized by a VHCF strength close to that of specimens without defects.

Fracture surfaces were investigated with the optical microscope. A peculiar fracture surface morphology was found in all the experimental failures. In particular, three characteristic regions, with different morphologies, were observed on the fracture surfaces. The first region, in which the fatigue crack originated, was characterized by an interfacial nature; whereas, the second (steadily crack propagation) and the third regions (final fracture) were characterized by a cohesive nature. The fracture surface morphologies of specimens with artificial defects were similar to the fracture surface morphology of specimens without defects, even in case of specimens with internal defects, thus confirming that the surface region is the most critical for the VHCF response.

Finally, the P-S-N curves were estimated and analyzed. Data points related to specimens without defects and to the specimen with internal defect were above the 1% P-S-N curve. Therefore, the 1% P-S-N curve was

conservatively considered as a design curve for the investigated butt-joint, provided that large macroscopic defects are not present.

To conclude, the experimental results confirmed that ultrasonic fatigue tests can be effectively carried out on structural adhesives with thickness up to $200\ \mu m$ and highlighted that, even in the VHCF region, surface plays a major role for crack nucleation.

Author Contributions: Andrea Tridello carried out the VHCF tests, analysed the VHCF test results, observed the fracture surfaces with the optical microscope and wrote the paper; Raffaele Ciardiello prepared the specimens, performed the static tests, observed the fracture surfaces with the Scanning Electron Microscope (SEM) and made additions to the paper; Davide S. Paolino has supervised the work and reviewed the full manuscript; Luca Goglio has supervised the work and reviewed the full manuscript.

REFERENCES

1 Banea MD, da Silva LFM. Adhesively bonded joints in composite materials: An overview. P. I. Mech. Eng. L.-J. Mat. 2009, 223: 1-18.

2 Rudawska A. Adhesive joint strength of hybrid assemblies: Titanium sheet-composites and aluminium sheet-composites—Experimental and numerical verification. Int. J. Adhes. Adhes. 2010; 30(7): 574-582.

3 Casalegno V, Salvo M, Rizzo S, Goglio L, Damiano O, Ferraris M. Joining of carbon fibre reinforced polymer to Al-Si alloy for space applications. Int. J. Adhes. Adhes. 2018; 82: 146-152.

4 Ciardiello R, Belingardi G, Martorana B, Brunella V. Physical and mechanical properties of a reversible adhesive for automotive applications. Int. J. Adhes. Adhes. 2019; 89: 117–128.

5 Jambor A, Beyer M. New cars-new materials. Mater. Design 1997; 18: 203-209.

6 Li Y., Lin Z., Jiang A., Chen G. Experimental study of glass-fiber mat thermoplastic material impact properties and lightweight automobile body analysis. Mater. Des. 2004; 25: 579-85.

7 da Silva LFM, Ochsner A, Adams RD. Handbook of Adhesion Technology. 1st Edition. Springer-Verlag Berlin Heidelberg; 2011.

8 Belingardi G, Chiandussi G. Stress flow in thin walled box beams obtained by adhesive bonding joining technology. Int. J. Adhes. Adhes. 2004; 24: 423–439.

9 Raftery GM, Harte AM, Rodd PD. Bonding of FRP materials to wood using thin epoxy gluelines. Int. J. Adhes. Adhes. 2009; 29: 580-588.

10 Imanaka M, Hamano T, Morimoto A, Ashino R, Kimoto M. Fatigue damage evaluation of adhesively bonded butt joints with a rubber modified epoxy adhesive. J. Adhes. Sci. Technol. 2003; 17:7: 981-994.

11 Banea MD, da Silva LFM, Carbas RJC, Cavalcanti DKK, De Souza LFG. The effect of environment and fatigue loading on the behaviour of TEPs-modified adhesives (In press). J Adhesion. doi.org/10.1080/00218464.2019.1680546

12 Bathias C, Paris PC. Gigacycle Fatigue in Mechanical Practice, 1st ed.; CRC Dekker, New York, USA, 2004.

13 Shanyavskiy AA. Very-High-Cycle-Fatigue of in-service air-engine blades, compressor and turbine. Sci. China Phys. Mech. Astron. 2014; 57: 19-29.

14 Tridello, A. VHCF response of Gaussian specimens made of high-strength steels: comparison between unrefined and refined AISI H13. Fatigue Fract. Engng. Mater. Struct. 2017; 40 (Issue 10): 1676–1689.

15 Tridello A., Paolino D.S., Chiandussi G., Rossetto M. Effect of electroslag remelting on the VHCF response of an AISI H13 steel. Fatigue Fract. Engng. Mater. Struct. 2017; 40 (Issue 11), 1783–1794.

16 Tridello A, Paolino DS, Chiandussi G, Goglio L. An innovative testing technique for assessing the VHCF response of adhesively bonded joints. Fatigue Fract. Engng. Mater. Struct. 2019; 42: 84–96.

17 Standard E1876–09 (2009). Standard test method for dynamic Young's modulus, shear modulus, and Poisson's ratio by impulse excitation of vibrations, ASTM Standard, West Conshohocken (PA).

18 Standard E756 – 05 (2017). Standard Test Method for Measuring Vibration-Damping Properties of Materials, ASTM Standard, West Conshohocken (PA).

19 Stanzl-Tschegg S. Very high cycle fatigue measuring techniques. Int. J. Fatigue 2014; 60, 2-17.

20 Mayer H. Recent developments in ultrasonic fatigue. Fatigue Fract. Eng. Mater. Struct. 2016; 39 (issue 1), 3-29.

21 Murakami S, Sekiguchi Y, Sato C, Yokoi E, Furusawa T. Strength of cylindrical butt joints bonded with epoxy adhesives under combined static or high-rate loading. Int. J. Adhes. Adhes. 2016; 67: 86-93.

22 Paolino DS, Chiandussi G, Rossetto M. A unified statistical model for S-N fatigue curves: probabilistic definition. Fatigue Fract. Eng. Mater. Struct. 2013; 36 (3): 187–201.